# 1

# New-Age Nano Adsorbents for Water Purification

*Subhadeep Biswas, Abhishek Johri, and Anjali Pal*

*Civil Engineering Department, Indian Institute of Technology Kharagpur, Kharagpur 721302, West Bengal, India*



## 1.1 Introduction

Rapid urbanization and huge industrialization often lead to the contamination of different water bodies. Irresponsible discharge of dyes, heavy metals, and emerging contaminants into the water often causes enormous pollution. A huge and uncontrolled release of unwanted materials into the water bodies deteriorates the water quality and poses a potential threat to aquatic life. The presence of colored substances, even in a trace quantity, in water is objectionable from an aesthetic point of view. Apart from that, many dye molecules show carcinogenicity and adverse toxic effects. In addition to this, illegal disposal of heavy metal ions present in industrial effluents has worsened the situation. In recent times, many harmful compounds, such as surfactants, phenol derivatives, and pharmaceutical waste, have also been detected in surface and subsurface water. These compounds are termed as emerging pollutants.

Considering all these facts, it is obvious that water purification is one of the most urgent needs to maintain the overall ecological balance. Innovative research activities are continuously carried out all over the globe on various wastewater treatment processes like adsorption, advanced oxidation process, electrocoagulation, electrooxidation, and membrane separation. Adsorption is one of the simplest and most efficient water and wastewater treatment techniques. However, the development of environmentally congenial adsorbents with excellent removal capacity and reusability is still a challenge. For a long time, activated carbon materials have been widely used for adsorption purposes. However, regeneration incapability and high cost associated with activated carbon materials are some of the major drawbacks in their use. Pristine materials like alumina, silica, and bentonite have also been explored in the recent past for adsorption purpose. Ma et al. [1] utilized bentonite-based adsorbents for removal of anionic pollutants from water bodies. Zhu et al. [2] in their recent review article highlighted the superiority of montmorillonite-based adsorbents for pollutant removal purposes. In this regard,

*Nanomaterials for Air and Water Purification*, First Edition.
Edited by Deepu A. Gopakumar, Jyotishkumar Parameswaranpillai, Jinu Jacob George, and Midhun Dominic C.D.

surface modifications, like acid modification, alkali modification, and surfactant modification, were also tried out for increasing adsorption capacity of different materials. Surfactant-modified alumina and silica have been found to be successful in removal of phenol [3], dyes [4, 5], and heavy metals [6].

In this field, nanomaterials have opened a new dimension for water treatment purpose. Nanoparticles are materials whose dimensions are less than 100 nm. In recent times, there has been a huge interest in the application of nanomaterials as adsorbents due to their excellent surface properties. Recently discovered materials like graphene and MXene have enhanced the scope of nanomaterials by forming compatible composites with them. Neha et al. [7] in their recent review article described the potential of different nanoadsorbents for the eradication of several toxic pharmaceutical compounds from water bodies. Kyzas and Matis documented in their review article the potential of various types of nanoadsorbents for wastewater treatment [8]. They highlighted the fact that the nanoadsorbents show unique physical and chemical characteristics, and the atoms that have high adsorption capacity lie on the surface of the nanomaterials. The current chapter describes the potential of different categories of nanoadsorbents such as metal–organic framework (MOF)-based nanoadsorbents, MXene-based nanoadsorbent, ZVI-based nanoadsorbent, and biochar-based nanoadsorbents for water purification purposes. Different mechanisms for pollutant removal by these nanoadsorbents have been elaborated. The next section deals with the characterization techniques commonly practiced in order to get insight into the adsorption process. Lastly, current challenges are often faced in this domain and the scope for further research has been presented before conclusion.

## 1.2 Different New-Age Nanoadsorbents

### 1.2.1 Metal–Organic Framework (MOF)-Based Nanoadsorbents

MOF-based compounds can be described as three-dimensional organic–inorganic complexes having porous structures, high specific surface area, and abundant sites exposed for adsorption [9]. In recent years, MOF-based nanocomposites have been explored by engineers and scientists worldwide for adsorption of different types of pollutants. A novel surfactant-functionalized MOF@MOF nanoadsorbent was reported by Li et al. [10] for Cr(VI) removal purposes. Thus, synthesized nanocomposite showed promising adsorption capacity and also reusability due to the presence of tunable pores along with abundant active sites on the surface. It showed good performance throughout a large pH range of 1–11, and the highest removal occurred at pH 2, with the maximum adsorption capacity being 932.1 mg $g^{-1}$. He et al. [11] carried out thermal decomposition of Ce-MOF micro and nanocomposites under $N_2$ atmosphere at a relatively lower temperature (400–500 °C). The composites thus produced after thermal treatment showed high phosphate removal efficiency. In comparison to ceria, the removal capacity was 2–4 times higher, and the maximum uptake was obtained at 189.4 mg $g^{-1}$. Yan et al. [12] reported the preparation and application of various polyoxometalates-MOF

nanocomposite for the removal of cationic dye methylene blue (MB). The removal occurred at 98% within five minutes for an initial MB concentration of 100 mg $l^{-1}$, and the maximum adsorption capacity obtained was 371 mg $g^{-1}$.

Soltani et al. [13] synthesized layered double hydroxide (LDH)-MOF nanocomposite without involvement of any toxic solvent and utilized the same for the remediation of heavy metals such as Cd(II) and Pb(II) from water. The LDH/MOF nanocomposite thus prepared showed promising performance toward heavy metal remediation, and the experimental data fitted well with the Langmuir isotherm model and pseudo-first-order kinetic model. The calculated maximum adsorption capacity of the nanocomposite was found to be 415.3 and 301.4 mg $g^{-1}$ toward the removal of Cd(II) and Pb(II), respectively. Yuan et al. [14] in their recent work designed a UiO-66-F-based nanocomposite for trapping carbamazepine from aqueous media. Experimental data fit well with the Langmuir isotherm model and pseudo-second-order kinetic model.

Nguyen et al. [15] reported the feasibility of application of zirconium-organic framework-based nanocomposites for the efficient adsorption of model cationic and anionic dyes MB and methyl orange (MO). The MOF-based nanoadsorbent showed excellent reusability for up to five cycles without any significant loss in uptake capacity.

Zr-based MOF nanocomposites have been explored by different research groups for wastewater treatment purpose. Huang et al. [16] used magnetic Zr-based nanocomposite $Fe_3O_4$@$SiO_2$@UiO-66 and its amino derivatives for the abatement of heavy metal ions and dyes from water bodies. It showed a high removal capacity for $Pb^{2+}$ (102 mg $g^{-1}$), MB (128 mg $g^{-1}$), and MO (219 mg $g^{-1}$). The nanoadsorbent has been reported to possess excellent selectivity toward anionic and cationic dyes by adjusting the solution pH. Moreover, it can completely remove both MO and MB at a neutral pH (~7). With respect to regeneration, it can be reused six times without losing efficiency. Some other MOF-based nanoadsorbents include Zr-cluster-based MOF for tetracycline removal [17], cobalt-MOF with morpholine for dye removal [18], and LDH/MOF nanocomposite for Orange II and Cr(VI) removal [19].

### 1.2.2 Graphene, Graphene Oxide (GO), and Reduced Graphene Oxide (rGO)-Based Nanoadsorbents

Carbon-based materials are often explored for adsorption purpose. In this regard, graphene is the latest member of the family of carbon allotropes. It is nearly one atom thick, has an excessively large surface-to- volume ratio, and is considered to be one of the most attractive new-age adsorbents. Besides graphene, graphene oxide (GO), reduced graphene oxide (rGO), and their composites also emerged as viable options of adsorbents. In one of the recent review articles, Kim et al. [20] investigated the potential of graphene-based nanocomposites for wastewater remediation. Possessing variable structure, chemical strength, and being light in density, the graphene family offers a numerous variety of nanocomposite materials for adsorption purpose. Shoushtarian et al. [21] explored the GO-based nanoadsorbent for efficient removal of Basic Red 46, a cationic dye. Under the

optimized condition, the maximum removal capacity reached up to 360 mg $g^{-1}$. The prepared GO was reused for four more cycles. However, the adsorption efficiency dropped with consecutive cycles. During four cycles of regeneration, the adsorption capacity dropped from 360 to 209 mg $g^{-1}$. Calimli et al. [22] reported the application of reduced GO-supported nano-Ni composite for the removal of MB. The maximum removal capacity was obtained at 946.12 mg $g^{-1}$.

ZnO nanoparticles coated with rGO were synthesized by Wang et al. [23] by means of self-assembly and in situ photoreduction technique. Thus synthesized rGO-based nanocomposite was utilized for the removal of rhodamine B (RhB) dye. rGO-supported ZnO nanocomposite showed excellent adsorption performance toward RhB removal. After adsorption, it was further subjected to dye photodegradation. In comparison to bare ZnO nanoparticles, rGO-supported nanoparticles showed much higher efficiency. Lujaniene et al. [24] explored the Prussian blue GO nanocomposite for the remediation of heavy metals and radionuclides from wastewater.

Verma and Dutta [25] synthesized nitrogen-enriched rGO-based nanocomposite for the removal of uranyl ions from water. A detailed experimental investigation showed that the adsorption process was kinetically and thermodynamically feasible. Removal occurred by chemisorption phenomenon, and the maximum uptake capacity reached up to 337.93 mg $g^{-1}$. High removal has been attributed to the large specific surface area of the nanocomposite (57.086 $m^2$ $g^{-1}$). El-Maghrabi et al. [26] reported the preparation and application of magnetic graphene-based nanocomposite for uranium removal. Excellent removal uptake of 455 mg $g^{-1}$ was exhibited by this nanocomposite within 60-minute contact time. Experimental data showed good correlation with pseudo-second-order kinetic model. Moreover, a high degree of sustainability has been shown by the nanocomposites (>5 times profiteering).

### 1.2.3 ZVI-Based Nanoadsorbents

nZVI is one of the most effective new-age adsorbents possessing several distinguished properties that immensely help in wastewater treatment. However, despite possessing several advantageous characteristics, it often gets agglomerated. Hence, various modifications have been reported in the literature to overcome this problem. Eljamal et al. [27] used four polymers, namely polyacrylamide, carboxymethyl cellulose, polyethylene sorbitan monolaurate, and polyvinylpyrrolidone, to increase the reactivity of nZVI and also to prevent their aggregation. Thus, different nanocomposites were finally deployed for nitrate and phosphorus removal from water. It was found that the combination of polyacrylamide and nZVI was the best for the adsorption of phosphorus.

Zhu et al. [28] applied activated carbon-loaded nZVI for the adsorptive removal of As(III) and As(V) from water. Activated carbon was loaded with ferrous sulfate, followed by reduction with $NaBH_4$. Arsenic removal was fast in the first 12 hours. However, equilibrium was reached at nearly 72 hours. It was seen during the interference study that the presence of different cations enhanced the removal of arsenate, but the presence of $Fe^{2+}$ diminished the uptake of arsenite. In order

to prevent the loss of reactivity of nZVI, Bui et al. [29] synthesized core/shell type structure of nZVI/manganese oxide nanocomposite and applied the same for arsenic remediation purpose. It was quite fascinating to observe that the nanocomposite thus produced was superior in adsorption capacity in comparison to the bare nZVI by two to three times. Jiang et al. [30] deployed biochar-supported nZVI for the removal of glyphosphate from water medium. Langmuir isotherm model fitted well with the experimental values, and the kinetic data fitted with the pseudo-second-order kinetic model. Hence, it was concluded that the adsorptive removal process involved both chemical and surface phenomena. Maximum adsorptive uptake capacity was noticed to be 80 mg $g^{-1}$, which is nearly twice that of biochar only. Thus loaded, nZVI improved adsorption capacity significantly.

For As(V) removal from wastewater in single-component system as well as in presence of Se(VI), Suazo-Hernandez et al. [31] deployed nZVI and nZVI- functionalized zeolite-based nanocomposites. Studies revealed that the zeolite-based nZVI composite was a much better option for arsenic remediation due to the presence of more specific sites on its surface.

Kadu and Chikate [32] prepared different clay-based nZVI nanocomposites for Cr(VI) removal purpose. The pore diffusion process has been found to be the governing mechanism for chromium abatement. Besides that, the presence of nZVI further facilitated the reduction of adsorbed hexavalent chromium.

### 1.2.4 Polysaccharide-Based Nanoadsorbents

Polysaccharides are biopolymers where complex carbohydrate molecules, i.e. long chain of monosaccharides, are linked by glycosidic bonds. They are biodegradable, nontoxic, biocompatible, low-cost, renewable, and sustainable, and they contain different functional groups. These polysaccharides have huge potential to be used as adsorbents in the field of wastewater treatment. These materials are popular as adsorbents due to their selectivity for pollutants and the capability of forming chelating compounds for trapping the pollutants using the –OH and $–NH_2$ groups present in their structure. In recent times, nanobiopolymers or nanocomposites with biopolymers have emerged as one of the most interesting materials for wastewater treatment. Different types of biopolymer-based nanocomposites that have been explored for wastewater treatment purpose have been described in the following section.

#### 1.2.4.1 Chitin and Chitosan-Based Adsorbents

Among the existing polysaccharides, chitin is the second most abundant polysaccharide after cellulose. It is an animal polysaccharide. It is obtained from crustacean (shells) as a byproduct. It is a homopolymer of β-(1-4) linked N-acetyl-D-glucosamine, and found in three forms: chitin-α, β, and γ. Chitosan (poliglusam) is obtained by deacetylation of chitin. It is made up of monomers of N-acetyl-D-glucosamine and D-acetyl-glucosamine linked by glycosidic β-(1-4) linkages. It is a cationic biopolymer, semicrystalline in nature and exists in solid state. It is insoluble in water and soluble in dilute acid. Solubility of chitosan

depends on many factors, such as degree of acetylation, concentration of acid, distribution of acetyl group on chitosan, molecular weight, and pH of solution.

Karimi et al. [33] deployed the chitosan/$Al_2O_3$/$Fe_3O_4$ nanocomposite for the removal of heavy metal ions such as Cd(II), Cu(II), Zn(II) from wastewater. In the case of Cd(II), the removal efficiency was highest, followed by Cu(II) and Zn(II). Hassan et al. [34] reported the application of chitosan/silica/ZnO nanocomposite for the removal of MB dye. Maximum removal capacity reached up to 293.3 mg $g^{-1}$ and the experimental data followed a pseudo-second-order kinetic model. Khan et al. [35] reported the application of chitosan/Co-silica nanocomposites for the removal of dyes such as MO, acridine orange, indigo carmine, and congo red (CR).

#### 1.2.4.2 Cellulose-Based Adsorbents

Cellulose is the most abundant naturally occurring biodegradable polysaccharide. It is a homopolymer made up of β-D-glucopyranose units linked by β-1,4 glycosidic linkages. It is semicrystalline in nature, showing both a crystalline and an amorphous nature depending upon the source of its extraction. Although it is nontoxic, renewable, biocompatible, sustainable, and cost-effective, it also has some demerits like poor hydrophilicity and low physical and chemical stability. These demerits can be overcome by reducing the size of polymers up to the nanometer. Reduction of polymer size results in availability of larger surface area, high strength, increased hydroxyl functional groups, and enhanced stability and stiffness of the polymer. Nanocellulose can be categorized into three groups on the basis of its extraction: as nanofibrillated cellulose (NFC), cellulose nanocrystal (CNC), and bacterial cellulose.

In order to remove Cr(VI) from aqueous medium, Dong et al. [36] explored CNC-based adsorbents. Polydopamine nanoparticles of size less than 30 nm were loaded on cellulose surface. Maximum uptake capacity toward Cr(VI) reached up to 205 mg $g^{-1}$, which is much higher in comparison to the cellulosic materials. Shoukat et al. [37] synthesized nanocomposites made up of bacterial cellulose and $TiO_2$. Thus prepared cellulose-based nanocomposite was explored for Pb(II) removal from wastewater. With initial concentration of lead at 100 mg $l^{-1}$, the removal efficiency reached 90% within 120 minutes at pH 7. The nanoadsorbent showed good reusability for three cycles.

#### 1.2.4.3 Starch-Based Adsorbents

Starch is a homopolysaccharide made up of glucose monomers linked through glycosidic linkages. It is found in plants, staple crops, crop seeds, and food items such as potatoes, rice, wheat, corn, and maize. It forms straight-chain polymer known as amylose as well as branched-chain polymer called as amylopectin. It is nontoxic, renewable, easily affordable, and biodegradable in nature. Different physical, chemical, genetic, and enzymatic methods are used for modification of starch. Chemical methods used for modification of starch are acid hydrolysis, cross linking, acetylation and esterification, oxidation, grafting, etc. Lawchoochaisakul et al. [38] reported the synthesis and application of cationic starch intercalated

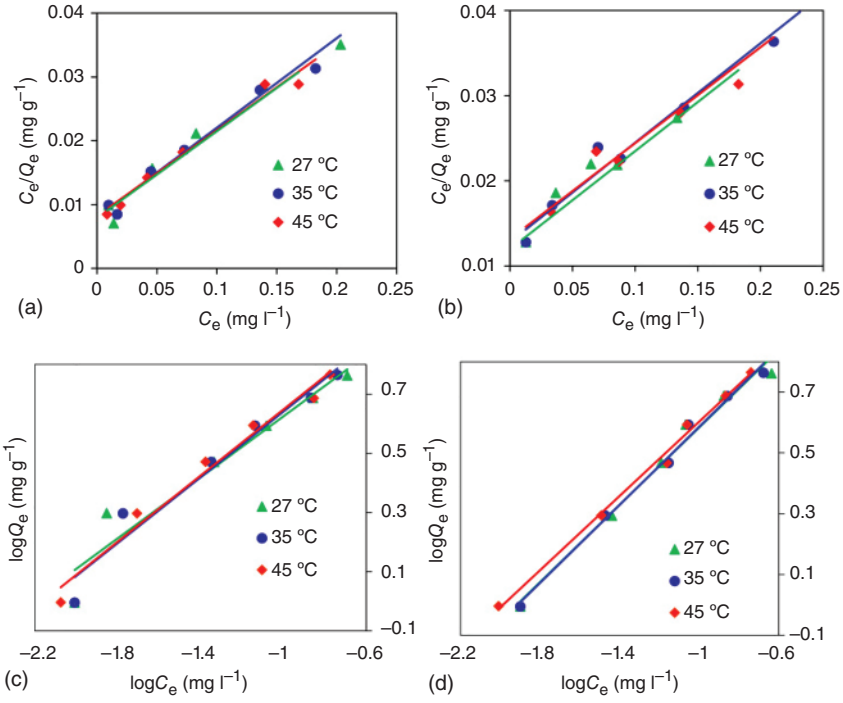


**Figure 1.1** Langmuir {(a) and (b)} and Freundlich {(c) and (d)} plots for As(III) uptake by C1 and C2, respectively. Source: Siddiqui et al. [39]/with permission of Elsevier.

montmorillonite nanocomposite for the treatment of dye wastewater. The presence of cationic starch in the nanocomposite enhanced the interlayer spacing, leading to an improvement in adsorption capacity. Siddiqui et al. [39] developed starch-functionalized maghemite nanocomposites for abatement of As(III) from dilute solutions in order to achieve potable water. Starch functionalized nanocomposite was designated as C1 and nonfunctionalized material was denoted as C2. Incorporation of starch in the maghemite enhanced adsorption capacity. Adsorption data fitted well with the Freundlich isotherm model as well as with the pseudo-second-order and film diffusion model. A graphical presentation of experimental data has been shown in Figure 1.1.

#### 1.2.4.4 Pectin-Based Adsorbents

Pectin is a plant-based linear polysaccharide found in cell walls of plants. It comprises monomers of galacturonic acid linked by α-(1-4) glycosidic linkage. The composition of pectin depends on the method of extraction from its sources. It is an anionic polymer containing hydroxyl and carboxyl groups present in its structure, which can be used as adsorption sites for removal of heavy metals and dyes. It shows gel-forming ability.

Babaladimath and Badalamoole [40] incorporated Ag nanoparticles inside the pectin hydrogel matrix to prepare a novel adsorbent for MB dye. Thus prepared

pectin-based nanocomposite showed much swelling due to the presence of Ag nanoparticles. After three cycles of usage, it showed promising performance, reaching 80% of its initial efficiency. Kodoth and Badalamoole [41] tested Ag nanoparticles embedded in pectin biopolymer nanocomposite for the adsorption of dyes and metal ions. The maximum adsorption capacity obtained was 1950 mg $g^{-1}$ for crystal violet (CV) dye, 111 mg $g^{-1}$ for Cu(II), and 130 mg $g^{-1}$ for Pb(II).

#### 1.2.4.5 Alginate-Based Adsorbents

Alginate is a natural copolymer made up of two epimer uronic acids, i.e. 1,4-(β-D) mannuronic acid (M) and 1,4- (α-L) guluronic acid (G). It is obtained from alginic acid, which is extracted from brown algae. It is biocompatible, nontoxic, highly water permeable, and used as a stabilizing agent for nanoparticles.

Alginate-based nanocomposites (alginate-clay, alginate-phosphate, and alginate-activated charcoal) were synthesized by Aziz et al. [42] for the removal of Cd(II) from wastewater. The highest adsorption efficiency was obtained by alginate-activated charcoal nanocomposites. For an initial concentration of Cd(II) equal to 1000 mg $l^{-1}$, the maximum adsorption capacity reached up to 137 mg $g^{-1}$. Moreover, due to its excellent stability and high removal capacity, it has been recommended for usage in continuous-flow real wastewater treatment systems. Majhi and Patra [43] described the applicability of nanocomposites synthesized from polyaniline and sodium alginate toward organic dye removal. Thus prepared alginate-based nanoadsorbents showed promising efficiency toward both cationic and anionic dyes. Mozaffari et al. [44], in their recent work, incorporated Cu(II) in an alginate-based hydrogel polymer matrix to prepare a novel nanocomposite useful for dye removal from wastewater. Malachite green (MG) and CV were tried out as the model dyes. Experimental data showed good fitting to the Freundlich isotherm model as well as to pseudo-second-order kinetic model. Moreover, one of the fascinating observations regarding this nanoadsorbent is that it showed good performance even after eight cycles.

### 1.2.5 MXene-Based Nanoadsorbents

MXenes are undoubtedly one of the most wonderful materials of recent times, possessing several promising qualities required for water treatment purpose. They are 2D carbides of transition metals with unique physicochemical properties, high hydrophilicity, and oxidation resistance. Moreover, cations can be intercalated through its layers. Jeon et al. [45] in their recent review highlighted the importance of MXene-based nanomaterials as one of the promising new-age adsorbents for pollution abatement purpose. Kim et al. [46] explored the adsorption capacity of $Ti_3C_2T_x$MXene for the removal of pharmaceutical compounds like amitriptyline, verapamil, carbamazepine, 17 α-ethinyl estradiol, ibuprofen, and diclofenac. It was observed that sonicated MXene nanocomposite exhibited better performance in comparison to the pristine MXene. Fard et al. [47] used 2D $Ti_3C_2T_x$ nanosheets for the adsorptive removal of barium from water bodies. Under optimized conditions, removal efficiency was achieved up to 90% within first ten minutes.

Sodium-intercalated $Ti_3C_2T_x$-based nanoadsorbent was explored by Ghani et al. [48] for the adsorptive removal of ciprofloxacin from wastewater. Sodium intercalated nanoadsorbent showed better removal efficiency in comparison to the pristine Mxene.

Jun et al. [49] explored the potency of the MXene-based adsorbent for elimination of radioactive $Cs^+$ from low-level radioactive wastewater. It showed an excellent adsorption capacity of 148 mg $g^{-1}$ within one hour. Moreover, the MXene-based adsorbent could be reused for at least four cycles, which undoubtedly makes it suitable for practical purpose.

Cai et al. [50] explored the potency of phytic acid-based MXene-based nanocomposites for the dye removal from sewage. MB and RhB were taken as the model dyes for the adsorption purpose. The nanocomposites showed excellent adsorptive removal capacity, and even after 12 cycles, MB removal efficiency remained at 85%. Shahzad et al. [51] deployed $MoS_2$-MXene nanocomposite for the adsorption of mercury. The maximum adsorption capacity reached 7.21 mmol $g^{-1}$.

### 1.2.6 Biochar-Based Nanoadsorbents

In the current decade, special attention has been paid to biochar-based composite materials for wastewater treatment purposes. Biochar refers to the class of organic substances that are produced by heating organic waste mass in presence of low oxygen or totally in absence of oxygen, which is termed as pyrolysis. The main purpose of producing biochar is to reduce the volume of waste and also produce energy. As they are resistant to degradation under ambient conditions, have large surface area, and possess negative surface charge, they are one of the most interesting classes of adsorbents for cationic pollutant removal from water bodies. Sizmur et al. [52] and Tang et al. [53] reviewed the application of biochar-based composites for wastewater treatment.

Liu et al. [54] reported the utility of biochar-supported carbon nanotubes and GO for the adsorption of Pb(II) and Cd(II) from water media. The adsorption capacity of the nanocomposite was higher than that of the bare biochar.

By means of ball milling, MgO/biochar nanocomposites were synthesized by Zheng et al. [55] and have been applied for the adsorptive removal of cationic dye and anionic phosphate from water medium. Li et al. [56] used agroforestry waste materials for the huge production of nano- and micro-sized biochar composites for several applications. Thus synthesized nanobiochar has been applied for $Pb^{2+}$ removal with varying initial concentrations (20–180 mg $l^{-1}$) at pH 7. The maximum adsorption capacities for upper and lower layer biochar have been reported as 55.56 and 41.67 mg $g^{-1}$, respectively. Shaikh et al. [57] prepared biochar-based nanocomposite consisting of doped AgNP and utilized it for the removal of toxic dyes from water bodies. Silver-doped biochar-based nanocomposite showed promising performance toward the removal of dyes like CR and RhB (>90%). Dye adsorption was found to be a spontaneous and exothermic process, and the experimental data fitted well with the Freundlich isotherm and pseudo-second-order model. Biochar-based nanocomposite was prepared by the

same research group [58] from waste tea leaves and explored for toxic dye removal from wastewater.

### 1.2.7 Hybrid Nanoadsorbents

In many cases, MOF, GO, Mxenes, biochars, and polysaccharides are often blended to produce nanocomposites of desired properties. Faradonbeh et al. [59] explored MOF-graphene hybrid nanocomposite for the purpose of Ni(II) removal from water media. For 300 ppm nickel solution, maximum removal efficiency reached up to 96% and the experimental data fitted well with the pseudo-second-order kinetic model. Among different hybrids prepared, maximum removal was observed for the nanohybrid synthesized by incorporating 30 wt% graphene into Cu-organic framework, and the highest capacity reached 1152 mg $g^{-1}$.

Hou et al. [60] utilized MOF (MIL-101 (Cr)) loaded nZVI composite for the removal of tetracycline antibiotic from water bodies. Maximum adsorption capacity of the nanocomposite was reported as 625 mg $g^{-1}$ and the experimental data fitted well with the pseudo-second-order kinetic model. Ventura et al. [61] synthesized novel hybrid nanoadsorbent composed of MOFs, $Fe_3O_4$, and GO. Hybrid nanoadsorbent thus produced was further applied for the removal of MB dye, and also tested for the adsorption of various metal ions such as $Na^+$, $Ca^{2+}$, $Mg^{2+}$, $SO_4^{2-}$, and $SiO_3^{2-}$ from a model brackish water. In comparison to the parent MOF material, the adsorption capacity toward MB increased by an amount of 30.52 and 13.75 mg $g^{-1}$ for the Co and Ni nanocomposites.

Mittal et al. [62] reported the application of hybrid nanocomposite made up of GO and xanthan gum toward CV removal. Thus prepared nanocomposite showed excellent performance toward CV removal with a maximum adsorption capacity of 1566.97 mg $g^{-1}$. Experimental data showed good correlation with Langmuir isotherm model and pseudo-second-order kinetic model.

To remove heavy metal ions such as Cu(II), Pb(II), and Cr(VI) from the water medium, Najafabadi et al. [63] applied chitosan/GO nanocomposite. It was revealed that the double exponential kinetic model and Redlich–Petersen isotherm best fit the experimental data. For Pb(II), Cu(II), and Cr(VI) the maximum adsorption capacity obtained was 461.3, 423.8, and 310.4 mg $g^{-1}$, respectively. Moreover, the nanocomposites could be reused without any loss of efficiency.

### 1.2.8 Other Nanoadsorbents

Apart from the above-mentioned nanocomposite materials, there are also other nanomaterials reported in the literature for pollutant removal. Abraham et al. [64] used the nanosize thorium(IV) metavandate for the removal of Ni(II) from water media. Kaolin and kaolin/ZnO nanocomposites have been explored by Mustapha et al. [65] for tannery wastewater treatment purpose. Nanocomposites were prepared by sol–gel method followed by wet impregnation technique. In comparison to kaolin, kaolin/ZnO nanocomposites showed better efficiency toward wastewater treatment. Under the same experimental conditions, Cr(VI) removal

**Table 1.1** List of some nanoadsorbents with their adsorption capacities.

| Adsorbent | Pollutant | Adsorption Capacity (mg $g^{-1}$) | Adsorption Isotherm Model | Reference |
|---|---|---|---|---|
| CTAB-surface-functionalized magnetic MOF@MOF | Cr (VI) | 932.1 | — | [10] |
| Ce – MOF- 500(S) | Phosphate | 189.4 | — | [11] |
| LDH/MOF nanocomposite | Cd (II) | 415.3 | Langmuir | [13] |
| | Pb (II) | 301.4 | | |
| Zr–MFC–N | Pb (II) | 102 | Langmuir | [16] |
| | MB | 128 | | |
| Zr–MFC–O | MO | 219 | | |
| GO nano adsorbent | BR 46 | 370.4 | Langmuir | [21] |
| Ni–rGO | MB | 946.12 | — | [22] |
| Amine- reduced graphene oxide nanocomposite (CARGO) | Uranyl ions | 337.93 | Langmuir | [25] |
| Magnetic ferberite graphene nanocomposite | U (VI) | 455 | Langmuir | [26] |
| nZVI/activated carbon | As (III) | 18.2 | Langmuir, Freundlich | [28] |
| | As (V) | 12 | | |
| nZVI/Mn oxide | As (III) | 29.4 | Langmuir | [29] |
| | As (V) | 35.7 | | |
| Biochar-nZVI | Glyphosate | 80 | Langmuir | [30] |
| Magnetic chitosan $Al_2O_3/Fe_3O_4$ nanocomposite | Cu (II) | 35.97 | Langmuir | [33] |
| | Cd (II) | 85.39 | | |
| | Zn (II) | 32.89 | | |
| Chitosan silica zinc oxide nanocomposite | MB | 293.3 | Langmuir | [34] |

*(Continued)*

**Table 1.1** (Continued)

| Adsorbent | Pollutant | Adsorption Capacity (mg $g^{-1}$) | Adsorption Isotherm Model | Reference |
|---|---|---|---|---|
| Polydopamine- coated cellulose nanocrystals | Cr (VI) | 205 | Langmuir | [36] |
| Cationic starch- intercalated montmorillonite | BB66<br>BY1 | 49.7<br>49.9 | Langmuir | [38] |
| Functionalized maghemite | As (III) | 8.6 | Freundlich | [39] |
| Pectin-based nanocomposite (Pec-*g*-PAMPS)<br>Pec-*g*-PAMPS-SN | MB | 62<br>89 | Freundlich | [40] |
| Pec-*g*-poly (AMPS-*co*-Aam)/Ag | CV<br>Cu (II)<br>Pb (II) | 1950<br>111<br>130 | Langmuir | [41] |
| Sodium alginate-based nanocomposite (SA-C Beads)<br>SA-P Beads<br>SA-Ch beads | Cd (II) | 112<br>105<br>137 | Langmuir | [42] |
| Polyaniline sodium nanocomposite | MB<br>RhB<br>O-II<br>MO | 555.5<br>434.78<br>476.19<br>416.66 | Langmuir | [43] |
| Nanocomposite hydrogel | MG<br>CV | — | Freundlich | [44] |
| Mxene | Ba | 9.3 | Freundlich | [47] |
| Mxene ($Ti_3C_2T_x$) | Cs | 148 | Freundlich | [49] |
| PA-Mxene-12 | MB<br>RhB | 42<br>22 | Langmuir | [50] |

| | | | | |
|---|---|---|---|---|
| Biochar-supported carbon nanotubes and GO nanocomposites | Pb (II)<br>Cd (II) | 38.6<br>10.8 | Dubinnin Radushke-vich | [54] |
| Biochar-based silver nanocomposite | RhB<br>CR | 23.39<br>23.55 | Freundlich | [57] |
| MOF–5Cu–Graphene hybrid 30% | Ni (II) | 1152 | Freundlich | [59] |
| nZVI/MIL–101(Cr) | TC | 625 | Langmuir | [60] |
| $Ni_3(BTC)_2$–MOF<br>$Co_3(BTC)_2$–MOF | MB | 67<br>54 | Langmuir | [61] |
| XG–HNC | CV | 1566.97 | Langmuir | [62] |
| Chitosan/graphene oxide nanofibrous adsorbent | Pb (II)<br>Cu (II)<br>Cr (VI) | 461.3<br>423.8<br>310.4 | Redlich -Peterson | [63] |
| Core shell bimagnetic NPs<br>$CoFe_2O_4$ @ γ $Fe_2O_3$ | P | 71.2 | Freundlich | [66] |
| Magnetite – maghemite nanoparticles | As (III)<br>As (V) | 3.69<br>3.71 | Freundlich | [68] |

by the nanocomposite was nearly 100% whereas it was around 78% with kaolin. The increase in treatment efficiency was due to the higher surface area of the nanocomposite.

Guerra et al. [66] utilized core@shell bimagnetic nanoparticles ($CoFe_2O_4$@γ-$Fe_2O_3$) for adsorptive removal of phosphorus from water. Two different-sized nanocomposites were prepared. Maximum adsorption capacity for the smaller-sized nanocomposite reached up to 71.2 mg $g^{-1}$ while it was 46.9 mg $g^{-1}$ for the bigger-sized nanocomposite at pH = 2.

Alias et al. [67] immobilized commercial $TiO_2$ and hydrothermally synthesized nano-flower like $TiO_2$ on basil seed support for dye adsorption purpose. Hydrothermally prepared nano$TiO_2$ composites exhibited better performance in comparison to the commercial ones. Moreover, after one cycle of use, when the nanocomposite was further subjected to reuse, its efficiency got enhanced significantly.

Chowdhury and Yanful [68] developed a useful and practical method for arsenic and chromium removal from water by using a mixture of maghemite and magnetite nanoparticles. In pH-controlled environment, almost all the arsenic and chromium species in the water were adsorbed. Maximum adsorption capacity was reported as 3.69 mg $g^{-1}$ for As(III), 3.71 mg $g^{-1}$ for As(V), and 2.4 mg $g^{-1}$ for Cr(VI) at pH 2, while their initial concentration in the solution was 1.5 mg $l^{-1}$ for As(III) and As(V) and 1 mg $l^{-1}$ for Cr(VI).

A list of recently reported nano adsorbents has been compiled in Table 1.1, along with their maximum adsorption capacities toward certain pollutants.

## 1.3 Different Mechanisms

Different interesting mechanisms have been put forward by different research groups regarding adsorption by nanocomposites. Adsorption of pollutants by the carbon material occurs through electrostatic and non-electrostatic interactions. Fard et al. [47] explained the mechanism of $Ba^{2+}$ removal by MXene-based nanoadsorbent. The removal occurred through physisorption as well as chemisorption. After the etching process, the surface of the MXene got covered with OH, F, and O groups. These groups enhanced the removal efficiency of barium. Furthermore, from D-R model it was clear that physisorption as well as chemisorption are involved in the removal process. Mechanisms can be well understood from Figure 1.2. Barium removal by MXene-based nanocomposite was proposed by the following two equations:

$$Ba^{2+} + 2OH^- \rightarrow Ba(OH)_2$$

$$Ba^{2+} + 2F^- \rightarrow BaF_2$$

Shaikh et al. [57] explained the CR uptake as surface complexation accompanied by electrostatic attraction. On the other hand, removal of RhB occurred only through surface complexation. The mechanism has been elucidated in Figure 1.3.

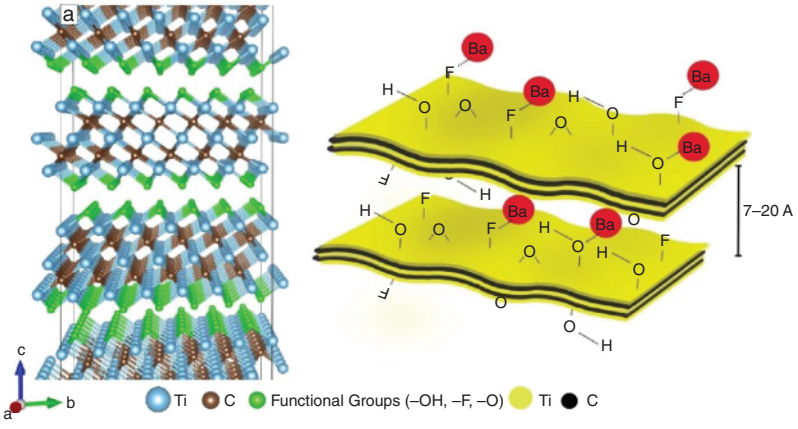


**Figure 1.2** Adsorption mechanism of barium ion on surface of MXene layers. Source: Fard et al. [47]/with permission of Elsevier.

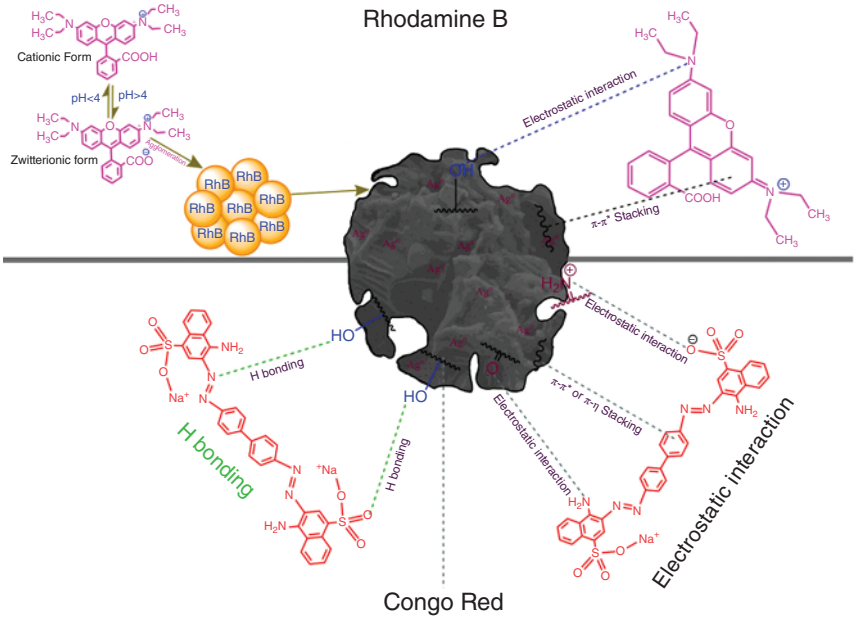


**Figure 1.3** Schematic illustration of probable RhB and CR adsorption mechanism using Ag-nBC. Source: Shaikh et al. [57]/with permission of Elsevier.

Mozaffari et al. [44] provided a detailed mechanism behind the dye uptake by their newly synthesized tetraamine Cu(II) nanoparticles embedded in a hydrogel matrix adsorbent termed as novel nanocomposite hydrogel (NCH). The nanoadsorbent worked well for CV and MG dye. Enhanced dye removal capacity was attributed due to the increase in surface area of the hydrogel composite owing to the incorporation of the nanoparticles. Considering $pK_a$ values of all the dyes taken for experimental purpose (CV, MG, RhB, CR, and MO), it was found that at pH 6, CV and MG existed as cationic form, RhB as neutral, and MO and CR as anionic form. On the other hand, hydrogel-based nanocomposite matrix existed as anion at pH 6. Therefore, cationic dyes got removed in greater percentages in comparison to the anionic dyes. For anionic dyes, only hydrogen bonding between the adsorbate and adsorbent was responsible for small removal percentage as shown in Figure 1.4.

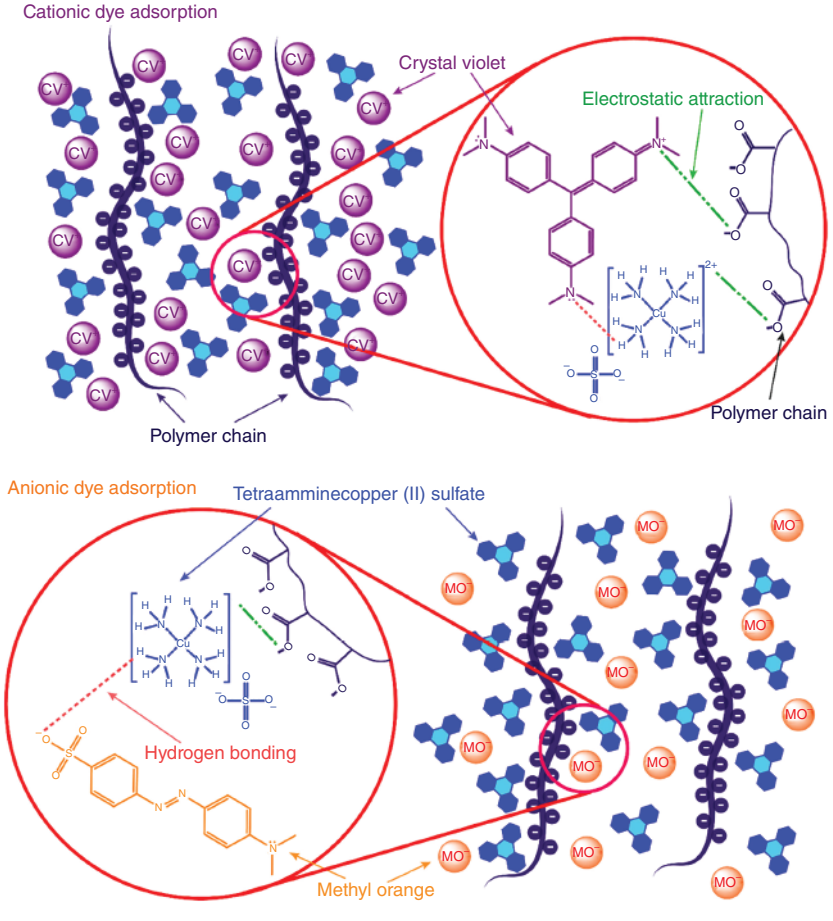


**Figure 1.4** Proposed electrostatic interaction and hydrogen bonding for dye adsorption by the NCH. Source: Mozaffari et al. [44]/with permission of Elsevier.

## 1.4 Different Characterization Techniques

### 1.4.1 FTIR Analysis

FTIR analyses are often done in order to get an idea of the functional groups involved in the adsorption phenomenon. Shaikh et al. [58] explained the dye removal by nanosilver modified biochar composites by FTIR analysis. From the FTIR analysis, it was clear that –OH, C ≡ N, and S=O groups were involved in the adsorption phenomenon. Furthermore, it was also confirmed that the C=C group on the surface of the nanocomposite contains a π-bond, which creates a π–π stacking with the delocalized π-aromatic bonds of RhB and CR molecules resulting in enhanced adsorption of these two dyes.

Das et al. [69] conducted FTIR analysis of GO/chitosan-PVA hydrogel nanocomposites. Strong peak at ∼3270 $cm^{-1}$ appeared due to the –OH functional group and $–NH_2$ group of chitosan. Peaks at ∼2939 and 1377 $cm^{-1}$ have been assigned corresponding to the C–H stretching vibration. Due to the reaction that occurred between hydroxyl groups of PVA and the $NH_2$ group of chitosan, C=N has been formed, and a peak has been obtained at ∼1647 $cm^{-1}$.

### 1.4.2 Electron Microscopic Analysis

In order to investigate the interesting morphological features of the nanoadsorbents, scanning electron microscopic (SEM) and transmission electron microscopic (TEM) analysis is often done. Jiang et al. [30] carried out the SEM and TEM analysis of biochar, bare nZVI and biochar-supported nZVI. It was observed that the surface of the original biochar was smooth consisting of lamellar multilayer structure of size around 0.5 μm. Bare nZVI was spherical in appearance with a size of 20–100 nm. After loading on the biochar surface, nZVI particles were uniformly dispersed and showed less sign of reunion. Moreover, the outer layer of the biochar-nZVI composite looked brown, possibly due to the oxidation. It prevented the interior nZVI from being oxidized and thus retained its reactivity.

From the SEM analysis of tea leaf-supported Ag nanoparticles [58], it was visualized that the surface of the nanocomposite exhibited porous, irregular surface with the presence of numerous cavities on it. It has been proposed that volatilization of lignin and holocellulose contributed to the pore formation, which ultimately aided in enhanced adsorption capacity of the nanoadsorbent.

In the work of Mozaffari et al. [44], TEM analysis showed that the size of the nanoparticles is within the range of 5–30 nm. From the TEM images of different weight percentages (0.5% and 0.7%) of chitosan/GO nanocomposite [63], it was clear that in 0.7% composite, GO sheets were embedded in the nanofibers, while in 0.5% composite, no such evidence was there.

### 1.4.3 X-Ray Diffraction (XRD) Analysis

Powder X-ray diffraction (XRD) is an analytical technique commonly practiced in order to determine the phase of a crystalline material and also to get an idea about

the oxidation state of the metal ions involved in the adsorption process. From the XRD spectrum of Co-MOF, it was found that the nanocomposites were crystalline in nature possessing lattice structure and unvarying morphology [18]. In the XRD spectrum of pristine GO [21], the diffraction peaks were obtained at $2\theta = 11.2°$ and 42.6° corresponding to (001) and (100) reflections, respectively.

In the work of Verma and Dutta [25], the XRD analysis confirmed the reduction of GO by L-cysteine. First, formation of GO from graphite was clear from the diffraction peak at $2\theta = 9.58°$ (corresponding to 002 plane of graphite), with an interplanar distance of 9.22 Å, which was larger than that of the graphite (3.34 Å). An increase in the d-spacing occurred due to the introduction of oxygen-containing moieties and water molecules between the graphene layers. Further introduction of L-cysteine amide shifted the diffraction peaks of the GO (of [002] plane) toward higher $2\theta$ value. A decrease in d spacing indicated reduction of GO.

### 1.4.4 UV-Diffuse Reflectance Spectra (DRS) Analysis

Diffuse reflectance spectroscopy is an advanced technique often explored for the determination of bandgap energy of nanoparticles. Abraham et al. [64] conducted DRS analysis of thorium metavandate nanoparticles. From the Tauc plot, the bandgap energy of the nanoparticles was found to be 2.36 eV. Mukherjee et al. [70] carried out the DRS study of $Cu^{2+}$ engrafted $MgAl_2O_4$ nanoparticles ($Mg_{1-x}Cu_xAl_2O_4$, $x = 0$, 0.1, 0.3, and 0.5). These nanocomposites are designated as MCA0, MCA1, MCA3, and MCA5. Strong peaks were noticed at wavelengths of 275, 280, and 236 nm, respectively. Moreover, a blue shift was observed in the spectra of the nanocomposites as the percentage of $Cu^{2+}$ increased due to the surface defects.

Arshadi [71] carried out the UV–Vis DRS analysis of Mn nanoparticles supported on mixed metal oxides (SA@MnNP) applied for Hg(II) removal purpose. Strong absorptions have been noticed at 253, 269, and 315 nm because of the occurrence of the $\pi \rightarrow \pi^*$, $n \rightarrow \pi^*$ transitions of the ligands. On the other hand, many low-intensity bands have been found in the visible region (500–700 nm), which may be due to $d \rightarrow d$ transitions for Mn(II)-Salen ligand interaction. DRS plot of the nanocomposite both before and after Hg(II) removal has been shown in Figure 1.5.

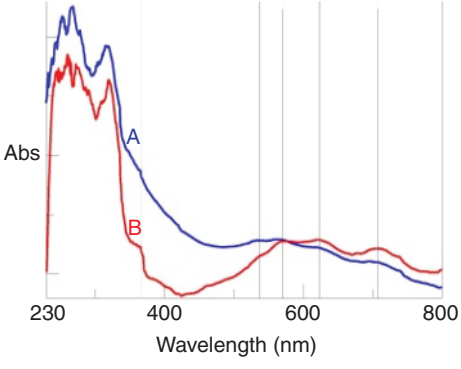


**Figure 1.5** UV–Vis diffuse reflectance spectra (DRS) of the Si/Al-PAEA = SA@MnNP before (A) and after adsorption of Hg(II) ions (B) from aqueous solution. Source: Arshadi [71]/with permission of Elsevier.

### 1.4.5 Brunauer–Emmett–Teller (BET) Analysis

Brunauer–Emmett–Teller (BET) analysis is often conducted to find out the specific surface area of nanocomposites. Shoushtarian et al. [21] found the specific surface area of pristine GO to be 465 $m^2$ $g^{-1}$.

Ahmad et al. [18] conducted the BET analysis of the MOF used for dye removal. $N_2$ adsorption–desorption isotherm indicated that it was a type IV isotherm and the BET surface area of the MOF was obtained as 153.45 $m^2$ $g^{-1}$. Verma and Dutta [25] carried out the BET analysis of the nanocomposite made up of rGO and L-cysteine amide (CARGO). Depending upon the ratio of the rGO and L-cysteine, the nanoadsorbents were named as CARGO-1, CARGO-2, and CARGO-3 with the increase of L-cysteine. Among the three, CARGO-1 possessed the highest specific area of 57.088 $m^2$ $g^{-1}$ followed by CARGO-2 and CARGO-3.

## 1.5 Current Challenges and Future Perspectives

Nanomaterials-based adsorbents are undoubtedly one of the most promising new-age materials for water purification. However, their applications often suffer from various drawbacks. Lata and Samadder described various challenges and drawbacks related to application of nanoadsorbents for arsenic remediation [72]. One of the most challenging aspects of using nanoadsorbents is the difficulty in their separation. Second, most of the nanoadsorbents are prepared via suspension and obtained as fine powders. However, these fine powders are not suitable as column materials as they possess low hydraulic conductivity.

Gomez-Pastora et al. [73], in their recent review article on the implementation of magnetic nanoparticles as adsorbents, described the pros and cons of applying nanoparticles as adsorbents. It was documented that the successful application of nanoadsorbent lay behind the regeneration capacity and also on the waste management technique of the spent solution used for regeneration. Moreover, it was also highlighted that the dose required by these nanoadsorbents was quite low in comparison to the other traditional adsorbents, and contact time was also relatively less. So, the apparent cost might look lesser for nanoadsorbent. But in some scenarios, the cost associated with the low-cost adsorbent might be lower than the nanoparticles. In one such report regarding the usage of nZVI, it was reported that the cost of commercially available nZVI oscillated from 225 to 2255 \$ $kg^{-1}$ [68]. It was much higher compared to that of the agro-waste-based adsorbents. Therefore, cost estimation for these nanoparticles should be optimized depending on the scenario.

Gusain et al. [74] in one of their recent review articles described the potency of carbon-based new-age nanoadsorbents for water purification. Apart from discussing several merits possessed by these nanocomposites, the authors highlighted several issues that need to be addressed seriously. Many carbon-based nanomaterials in their pristine form often fail to serve the desired purpose. Prone to segregation, fouling effects and poor adsorption capacities are often encountered with those materials. However, these problems can be handled by means of synthesizing

macroscopic structure containing carbon nanomaterials as the building blocks. But these macrostructure or superstructures often suffer from poor mechanical strength. Hence, reinforcement with nanofibers, crosslinking with other reagents, or embedding in the polymer matrix are often carried out.

In most of the studies, nanomaterials are applied for small-scale study. However, large-scale studies in real wastewater scenario are extremely necessary from practical point of view. In addition to this, environmental impact assessment of application of these nanoadsorbents should be thoroughly done. Understanding the fate and transport of these nanoparticles are essential, as after adsorption the pollutant-loaded nanoparticles may affect the ecological system in a negative manner.

Hence, this chapter discusses the positive aspects of different kinds nanoadsorbents that are often used for wastewater treatment. Different modifications and several mechanisms are discussed. Finally, some recommendations are highlighted for carrying out future research in this field.

## Acknowledgment

The authors are grateful to IIT Kharagpur and Ministry of Education, Government of India, for providing financial support.

## Conflicts of Interest

The authors declare no conflict of interest.

## References

1 Ma, J., Qi, J., Yao, C. et al. (2012). A novel bentonite-based adsorbent for anionic pollutant removal from water. *Chem. Eng. J.* 200–202: 97–103.
2 Zhu, R., Chen, Q., Zhou, Q. et al. (2016). Adsorbents based on montmorillonite for contaminant removal from water: a review. *Appl. Clay Sci.* 123: 239–258.
3 Adak, A., Pal, A., and Bandyopadhyay, M. (2006). Removal of phenol from water environment by surfactant-modified alumina through adsolubilization. *Colloids Surf., A* 277: 63–68.
4 Adak, A., Bandyopadhyay, M., and Pal, A. (2005). Removal of crystal violet dye from wastewater by surfactant-modified alumina. *Sep. Purif. Technol.* 44: 139–144.
5 Koner, S., Pal, A., and Adak, A. (2010). Cationic surfactant adsorption on silica gel and its application for wastewater treatment. *Desalin. Water Treat.* 22: 1–8.
6 Khobragade, M.U. and Pal, A. (2014). Investigation on the adsorption of Mn(II) on surfactant-modified alumina: batch and column studies. *J. Environ. Chem. Eng.* 2: 2295–2305.

7 Neha, R., Adithya, S., Jayaraman, R.S. et al. (2021). Nanoadsorbents an effective adsorbent for removal of toxic pharmaceutical compounds from aqueous environment: a critical review on emerging trends. *Chemosphere* 272: 129852.

8 Kyzas, G.Z. and Matis, K.A. (2015). Nanoadsorbents for pollutant removal: a review. *J. Mol. Liq.* 203: 159–168.

9 Joseph, L., Jun, B., Jang, M. et al. (2019). Removal of contaminants of emerging concern by metal-organic framework nanoadsorbents: a review. *Chem. Eng. J.* 369: 928–946.

10 Li, L., Xu, Y., Zhong, D., and Zhong, N. (2020). CTAB-surface-functionalized magnetic MOF@MOF composite adsorbent for Cr(VI) efficient removal from aqueous solution. *Colloids Surf. A.* 586: 124255.

11 He, J., Xu, Y., Wang, W. et al. (2020). Ce(III) nanocomposites by partial thermal decomposition of Ce-MOF for effective phosphate adsorption in a wide pH range. *Chem. Eng. J.* 379: 122431.

12 Yan, A., Yao, S., Li, Y. et al. (2014). Incorporating polyoxometalates into a porous MOF greatly improves its selective adsorption of cationic dyes. *Chem. Eur. J.* 20: 6927–6933.

13 Soltani, R., Pelalak, R., Pishnamazi, M. et al. (2021). A novel and facile green synthesis method to prepare LDH/MOF nanocomposite for removal of Cd(II) and Pb(II). *Sci. Rep.* 11: 1609.

14 Yuan, N., Gong, X., and Han, B. (2021). Hydrophobic fluorous metal-organic framework nanoadsorbent for removal of hazardous wastes from water. *ACS Appl. Nano Mater.* 4: 1576–1585.

15 Nguyen, L.H.T., Nguyen, H.T.T., Le, B.Q.G. et al. (2021). Microwave-assisted solvothermal synthesis of defective zirconium-organic framework as a recyclable nano-adsorbent with superior adsorption capacity for efficient removal of toxic organic dyes. *Colloid Interf. Sci. Commun.* 46: 100511.

16 Huang, L., He, M., Chen, B., and Hu, B. (2018). Magnetic Zr-MOFs nanocomposites for rapid removal of heavy metal ions and dyes from water. *Chemosphere* 199: 435–444.

17 Fu, M., Deng, X., Wang, S. et al. (2022). Scalable robust nano-porous Zr-based MOF adsorbent with high-capacity for sustainable water purification. *Sep. Purif. Technol.* 288: 120620.

18 Ahmad, K., Shah, H., Parveen, S. et al. (2021). Metal Organic Framework (KIUB-MOF-1) as efficient adsorbent for cationic and anionic dyes from brackish water. *J. Mol. Struct.* 1242: 130898.

19 Soltani, R., Marjani, A., and Shirazian, S. (2020). A hierarchial LDH/MOF nanocomposite: single, simultaneous and consecutive adsorption of a reactive dye and Cr(VI). *Dalton Trans.* 49: 5323–5335.

20 Kim, S., Park, C.M., Jang, M. et al. (2018). Aqueous removal of inorganic and organic contaminants by graphene-based nanoadsorbents: a review. *Chemosphere* 212: 1104–1124.

21 Shoushtarian, F., Moghaddam, M.R.A., and Kowsari, E. (2020). Efficient regeneration/reuse of graphene oxide as a nanoadsorbent for removing basic Red 46 from aqueous solutions. *J. Mol. Liq.* 312: 113386.

**22** Calimli, M.H., Nas, M.S., Burhan, H. et al. (2020). Preparation, characterization and adsorption kinetics of methylene blue dye in reduced-graphene oxide supported nanoadsorbents. *J. Mol. Liq.* 309: 113171.

**23** Wang, J., Tsuzuki, T., Tang, B. et al. (2012). Reduced graphene oxide/Zno composite: reusable adsorbent for pollutant management. *ACS Appl. Mater. Interfaces* 4: 3084–3090.

**24** Lujaniene, G., Semcuk, S., Lecinskyte, A. et al. (2017). Magnetic graphene oxide based nano-composites for removal of radionuclides and metals from contaminated solutions. *J. Environ. Radioact.* 166: 166–174.

**25** Verma, S. and Dutta, R.K. (2017). Development of cysteine amide reduced graphene oxide (CARGO) nano-adsorbents for enhanced uranyl ions removal from aqueous medium. *J. Environ. Chem. Eng.* 5: 4547–4558.

**26** El-Maghrabi, H.H., Abdelmaged, S.M., Nada, A.A. et al. (2017). Magnetic graphene based nanocomposite for uranium scavenging. *J. Hazard. Mater.* 322: 370–379.

**27** Eljamal, R., Eljamal, O., Maamoun, I. et al. (2020). Enhancing the characteristic and reactivity of nZVI: polymers effect and mechanisms. *J. Mol. Liq.* 315: 113714.

**28** Zhu, H., Jia, Y., Wu, X., and Wang, H. (2009). Removal of arsenic from water by supported nano zero-valent iron on activated carbon. *J. Hazard. Mater.* 172: 1591–1596.

**29** Bui, T.H., Kim, C., Hong, S.P., and Yoon, J. (2017). Effective adsorbent for arsenic removal: core/shell structural nano zero-valent iron/manganese oxide. *Environ. Sci. Pollut. Res.* 24: 24235–24242.

**30** Jiang, X., Ouyang, Z., Zhang, Z. et al. (2018). Mechanism of glyphosphate removal by biochar supported nano-zero-valent iron in aqueous solutions. *Colloids Surf., A* 547: 64–72.

**31** Suazo-Hernandez, J., Sepulveda, P., Manquian-Cerda, K. et al. (2019). Synthesis and characterization of zeolite-based composites functionalized with nanoscale zero-valent iron for removing arsenic in the presence of selenium from water. *J. Hazard. Mater.* 373: 810–819.

**32** Kadu, B.S. and Chikate, R.C. (2013). nZVI based nanocomposites: role of noble metal and clay support on chemisorptive removal of Cr(VI). *J. Environ. Chem. Eng.* 1: 320–327.

**33** Karimi, F., Ayati, A., Tanhaei, B. et al. (2022). Removal of metal ions using a new magnetic chitosan nano bio-adsorbent; a powerful approach in water treatment. *Environ. Res.* 203: 111753.

**34** Hassan, H., Salama, A., El-ziaty, A.K., and El-Sakhawy, M. (2019). New chitosan/silica/zinc oxide nanocomposite as adsorbent for dye removal. *Int. J. Biol. Macromol.* 131: 520–526.

**35** Khan, S.A., Khan, S.B., Kamal, T. et al. (2016). Antibacterial nanocomposites based on chitosan/Co-MCM as a selective and efficient adsorbent for organic dyes. *Int. J. Biol. Macromol.* 91: 744–751.

**36** Dong, L., Deng, R., Xiao, H. et al. (2019). Hierarchial polydopamine coated cellulose nanocrystal microstructures as efficient nanoadsorbents for removal of Cr(VI) ions. *Cellulose* 26: 6401–6414.

**37** Shoukat, A., Wahid, F., Khan, T. et al. (2019). Titanium oxide-bacterial cellulose bioadsorbent for the removal of lead ions from aqueous solution. *Int. J. Biol. Macromol.* 129: 965–971.

**38** Lawchoochaisakul, S., Monvisade, P., and Siriphannon, P. (2021). Cationic starch intercalated montmorillonite nanocomposites as natural based adsorbent for dye removal. *Carbohydr. Polym.* 253: 117230.

**39** Siddiqui, S.I., Singh, P.N., Tara, N. et al. (2020). Arsenic removal from water by starch functionalized maghemite nano-adsorbents: thermodynamics and kinetics investigations. *Colloid Interf. Sci.* 36: 100263.

**40** Babaladimath, G. and Badalamoole, V. (2019). Silver nanoparticles embedded pectin-based hydrogel: a novel adsorbent material for separation of cationic dyes. *Polym. Bull.* 76: 4215–4236.

**41** Kodoth, A.K. and Badalamoole, V. (2020). Silver nanoparticle-embedded pectin-based hydrogel for adsorptive removal of dyes and metal ions. *Polym. Bull.* 77: 541–564.

**42** Aziz, F., Achaby, M.E., Lissaneddine, A. et al. (2020). Composites with alginate beads: a novel design of nano-adsorbents impregnation for large scale continuous flow wastewater treatment pilots. *Saudi. J. Biol. Sci.* 27: 2499–2508.

**43** Majhi, D. and Patra, B.N. (2020). Polyaniline and sodium alginate nanocomposite; a pH-responsive adsorbent for the removal of organic dyes from water. *RSC Adv.* 10: 43904–43914.

**44** Mozaffari, T., Vanashi, A.K., and Ghasemzadeh, H. (2021). Nanocomposite hydrogel based on sodium alginate, poly (acrylic acid), and tetraamminecopper(II) sulfate as an efficient dye adsorbent. *Carbohydr. Polym.* 267: 118182.

**45** Jeon, M., Jun, B., Kim, S. et al. (2020). A review on MXenes-nanomaterials as adsorbents in aqueous solution. *Chemosphere* 261: 127781.

**46** Kim, S., Gholamirad, F., Yu, M. et al. (2021). Enhanced adsorption performance for selected pharmaceutical compounds by sonicated $Ti_3C_2T_x$MXene. *Chem. Eng. J.* 406: 126789.

**47** Fard, A.K., Mckay, G., Chamoun, R. et al. (2017). Barium removal from synthetic natural and produced water using MXene as two dimensional (2-D) nanosheet adsorbent. *Chem. Eng. J.* 317: 331–342.

**48** Ghani, A.A., Shahzad, A., Moztahida, M. et al. (2021). Adsorption and electrochemical regeneration of intercalated $Ti_3C_2T_x$ MXene for the removal of ciprofloxacin from wastewater. *Chem. Eng. J.* 421: 127780.

**49** Jun, B., Jang, M., Park, C.M. et al. (2020). Selective adsorption of $Cs^+$ by MXene ($Ti_3C_2T_x$) from model low-level radioactive wastewater. *Nucl. Eng. Technol.* 52: 1201–1207.

**50** Cai, C., Wang, R., Liu, S. et al. (2020). Synthesis of self-assembled phytic acid-MXene nanocomposites via a facile hydrothermal approach with elevated dye adsorption capacities. *Colloids Surf., A* 589: 124468.

**51** Shahzad, A., Jang, J., Lim, S., and Lee, D.S. (2020). Unique selectivity and rapid uptake of molybdenum-disulphide-functionalized MXene nanocomposite for mercury adsorption. *Environ. Res.* 182: 109005.

**52** Sizmur, T., Fresno, T., Akgul, G. et al. (2017). Biosorption modification to enhance sorption of inorganics from water. *Bioresour. Technol.* 246: 33–47.

**53** Tan, X., Liu, Y., Gu, Y. et al. (2016). Biochar-based nano-composites for the decontamination of wastewater: a review. *Biresour. Technol.* 212: 318–333.

**54** Liu, T., Gao, B., Fang, J. et al. (2016). Biochar-supported carbon nanotube and graphene oxide nanocomposites for Pb(II) and Cd(II) removal. *RSC Adv.* 6: 24314–24319.

**55** Zheng, Y., Wan, Y., Chen, J. et al. (2020). MgO modified biochar produced through ball milling: a dual-functional adsorbent for removal of different contaminants. *Chemosphere* 243: 125344.

**56** Li, L., Zhang, K., Chen, L. et al. (2017). Mass preparation of micro/nano-powders of biochar with water-dispersibility and their potential application. *New J. Chem.* 41: 9649–9657.

**57** Shaikh, W.A., Islam, R.U., and Chakraborty, S. (2021). Stable silver nanoparticle doped mesoporous biochar-based nanocomposite for efficient removal of toxic dyes. *J. Environ. Chem. Eng.* 9: 104982.

**58** Shaikh, W.A., Kumar, A., Chakraborty, S. et al. (2022). Biochar-based nanocomposite from waste tea leaf for toxic dye removal: from facile fabrication to functional fitness. *Chemosphere* 291: 132788.

**59** Faradonbeh, M.R., Dadkhah, A.A., Rashidi, A. et al. (2018). Newly MOF-graphene hybrid nanoadsorbent for removal of Ni(II) from aqueous phase. *J. Inorg. Organomet. Polym. Mater.* 28: 829–836.

**60** Hou, X., Shi, J., Wang, N. et al. (2020). Removal of antibiotic tetracycline by metal-organic framework MIL-101 (Cr) loaded nano zero-valent iron. *J. Mol. Liq.* 313: 113512.

**61** Ventura, K., Arrieta, R.A., Marcos-Hernandez, M. et al. (2020). Superparamagnetic MOF@GO Ni and Co based hybrid nanocomposites as efficient water adsorbents. *Sci. Total Environ.* 738: 139213.

**62** Mittal, H., Alili, A.A., Morajkar, P.P., and Alhassan, S.M. (2021). Graphene oxide crosslinked hydrogel nanocomposites of xanthan gum for the adsorption of crystal violet dye. *J. Mol. Liq.* 323: 115034.

**63** Najafabadi, H.H., Irani, M., Rad, L.R. et al. (2015). Removal of $Cu^{2+}$, $Pb^{2+}$ and $Cr^{6+}$ from aqueous solutions using a chitosan/graphene oxide composite nanofibrous adsorbent. *RSC Adv.* 5: 16532–16539.

**64** Abraham, S.D., Bennie, R.B., Joel, C. et al. (2020). Synthesis and microstructural analysis of nanosized $Th(VO_3)_4$ for the uptake of Ni(II) ions from aqueous solution. *Sep. Sci. Technol.* 55: 247–256.

**65** Mustapha, S., Tijani, J.O., Ndamitso, M.M. et al. (2020). The role of kaolin and kaolin/ZnO nanoadsorbent in adsorption studies for tannery wastewater treatment. *Sci. Rep.* 10: 13068.

**66** Guerra, A.A.A.M., Campos, A.F.C., Lima, R.M. et al. (2020). Efficient uptake of phosphorus from water by core@shell bimagnetic nanoadsorbents. *J. Environ. Chem. Eng.* 8: 103888.

**67** Alias, S.S., Harun, Z., Azhar, F.H. et al. (2020). Comparison between commercial and synthesised nano flower-like rutile $TiO_2$ immobilised on green super adsorbent towards dye wastewater treatment. *J. Cleaner Prod.* 251: 119448.

**68** Chowdhury, S.R. and Yanful, E.K. (2010). Arsenic and chromium removal by mixed magnetite-maghemite nanoparticles and the effect of phosphate on removal. *J. Environ. Manage.* 91: 2238–2247.

**69** Das, L., Das, P., Bhowal, A., and Bhattacharjee, C. (2020). Synthesis of hybrid hydrogel nano-polymer composite using graphene oxide, chitosan and PVA and its application in wastewater treatment. *Environ. Technol. Innov.* 2020: 100664.

**70** Mukherjee, A., Adak, M.K., Dhak, P., and Dhak, D. (2020). A simple chemical method for the synthesis of $Cu^{2+}$ engrafted $MgAl_2O_4$ nanoparticles: efficient fluoride adsorbents, photocatalyst and latent finger print detection. *J. Environ. Sci.* 88: 301–315.

**71** Arshadi, M. (2015). Manganese chloride nanoparticles: a practical adsorbent for the sequestration of Hg(II) ions from aqueous solution. *Chem. Eng. J.* 259: 170–182.

**72** Lata, S. and Samadder, S.R. (2016). Removal of arsenic from water using nano adsorbents and challenges: a review. *J. Environ. Manage.* 166: 387–406.

**73** Gomez-Pastora, J., Bringas, E., and Ortiz, I. (2014). Recent progress and future challenges on the use of high performance magnetic nano-adsorbents in environmental applications. *Chem. Eng. J.* 256: 187–204.

**74** Gusain, R., Kumar, N., and Ray, S.S. (2020). Recent advances in carbon nanomaterial-based adsorbents for water purification. *Coord. Chem. Rev.* 45: 213111.